

Prospects for Higgs Searches via VBF at the LHC with the ATLAS Detector

K. Cranmer, Y.Q. Fang, B. Mellado, S. Paganis, W. Quayle and Sau Lan Wu

Abstract

We report on the potential for the discovery of a Standard Model Higgs boson with the vector boson fusion mechanism in the mass range $115 < M_H < 500$ GeV with the ATLAS experiment at the LHC. Feasibility studies at hadron level followed by a fast detector simulation have been performed for $H \rightarrow W^{(*)}W^{(*)} \rightarrow l^+l^- \cancel{p}_T$, $H \rightarrow \gamma\gamma$ and $H \rightarrow ZZ \rightarrow l^+l^-q\bar{q}$. The results obtained show a large discovery potential in the range $115 < M_H < 300$ GeV. Results obtained with multivariate techniques are reported for a number of channels.

1. Introduction

In the Standard Model (SM) of electro-weak and strong interactions, there are four types of gauge vector bosons (gluon, photon, W and Z) and twelve types of fermions (six quarks and six leptons) [1, 2, 3, 4]. These particles have been observed experimentally. The SM also predicts the existence of one scalar boson, the Higgs boson [5, 6, 7, 8, 9, 10]. The observation of the Higgs boson remains one of the major cornerstones of the SM. This is a primary focus of the ATLAS Collaboration [11].

The Higgs at the LHC is produced predominantly via gluon-gluon fusion [12]. For Higgs masses, M_H , such that $M_H > 100$ GeV, the second dominant process is vector boson fusion (VBF) [13, 14].

Early analyses performed at the parton level with the decays $H \rightarrow W^{(*)}W^{(*)}$, $\tau^+\tau^-$ and $\gamma\gamma$ via VBF indicated that this mechanism could produce strong discovery modes in the range of the Higgs mass $115 < M_H < 200$ GeV [15, 16, 17, 18]. The ATLAS collaboration has performed feasibility studies for these decay modes including more detailed detector description and the implementation of initial-state and final-state parton showers (IFSR), hadronization and multiple interactions [19].

Here, we present an update of the potential of observing the Higgs boson via VBF with $H \rightarrow W^{(*)}W^{(*)} \rightarrow l^+l^- \cancel{p}_T$, where \cancel{p}_T stands for missing transverse momentum carried by neutrinos, reported in [19]. This analysis has been extended to larger Higgs masses. Also, we investigated the prospects of observing a SM Higgs boson with $H \rightarrow \gamma\gamma$ and $H \rightarrow ZZ \rightarrow l^+l^-q\bar{q}$. Results obtained with multivariate techniques are reported for a number of channels. Finally, the status of the overall SM Higgs discovery potential of the ATLAS detector is presented.

2. Experimental Signatures

The VBF mechanism displays a number of distinct features, which may be exploited experimentally to suppress SM backgrounds: Higgs decay products are accompanied by two energetic forward jets originating from incoming quarks and suppressed jet production in the central region is expected due to the lack of color flow between the initial state quarks. In this paper, tagging jets are defined as the highest and next highest transverse momentum, P_T , jets in the event. A number of variables were used in the VBF analyses reported in this paper: P_T of the leading and the sub-leading jets, P_{Tj_1} and P_{Tj_2} , pseudorapidity, η , of the leading and sub-leading jets, η_{j_1} and η_{j_2} , with $\Delta\eta_{j_1j_2} = |\eta_{j_1} - \eta_{j_2}|$, the difference of tagging jets' azimuthal angles, $\Delta\phi_{j_1j_2}$ and tagging jets' invariant mass, $M_{j_1j_2}$. The tagging jets are required to be in opposite hemispheres ($\eta_{j_1}\eta_{j_2} < 0$).

In Sections 4. and 6. a number of variables are used: pseudorapidity and azimuthal angle difference between leptons, η_{ll} and ϕ_{ll} , and di-lepton invariant mass, M_{ll} . In Section 5. the following variables are used: P_T of the leading and sub-leading γ 's, $P_{T\gamma_1}$ and $P_{T\gamma_2}$, pseudorapidity and azimuthal angle difference between γ 's, $\eta_{\gamma\gamma}$ and $\phi_{\gamma\gamma}$, and di- γ invariant mass, $M_{\gamma\gamma}$.

m_H	(GeV)	120	130	140	150	160	170	180
$\sigma(q\bar{q}H)$	(pb)	4.29	3.97	3.69	3.45	3.19	2.95	2.80
$\sigma \cdot BR(H \rightarrow W^{(*)}W^{(*)})$	(fb)	522	1107	1771	2363	2887	2850	2618
$\sigma \cdot BR(H \rightarrow \gamma\gamma)$	(fb)	9.38	8.89	7.14	4.76	1.71	-	-

Table 1: Total vector boson fusion production cross-sections, $\sigma(q\bar{q}H)$, $\sigma \cdot BR(H \rightarrow W^{(*)}W^{(*)})$ and $\sigma \cdot BR(H \rightarrow \gamma\gamma)$ for a low mass Higgs. The cross-sections have been computed using the CTEQ5L structure function parametrization.

m_H	(GeV)	190	200	250	300	350	400	450	500
$\sigma(q\bar{q}H)$	(pb)	2.58	2.44	1.82	1.38	1.06	0.83	0.66	0.53
$\sigma \cdot BR(H \rightarrow WW)$	(fb)	2005	1793	1276	954	721	488	363	289
$\sigma \cdot BR(H \rightarrow ZZ)$	(fb)	562	637	542	424	332	227	172	138

Table 2: Total vector boson fusion production cross-sections, $\sigma \cdot BR(H \rightarrow WW)$ and $\sigma \cdot BR(H \rightarrow ZZ)$ for a heavier Higgs. The cross-sections have been computed using the CTEQ5L structure function parametrization.

The following decay chains have been considered in the analysis: $H \rightarrow W^{(*)}W^{(*)} \rightarrow l^+l^-p_T$, $H \rightarrow \gamma\gamma$ and $H \rightarrow ZZ \rightarrow l^+l^-q\bar{q}$. A number of relevant experimental aspects have been addressed in detail in [11, 19] and will not be touched upon in this work: triggering, lepton and photon identification, fake lepton and photon rejection, jet tagging, central jet veto and b-jet veto efficiencies.¹

3. Signal

The Born level cross-sections for the VBF process have been calculated using the PYTHIA package [20, 21].² The results are given in Tables 1-2 for different Higgs masses. The signal (and background) Born level cross-sections have been computed using the CTEQ5L structure function parametrization [23]. The products of the signal cross-sections and the branching ratios of the Higgs boson into $W^{(*)}W^{(*)}$, $\gamma\gamma$, and ZZ , which have been calculated using the programme HDECAY [24], are also included in Table 1-2.

The impact of initial and final state QCD radiation, hadronization, multiple interactions and underlying event were simulated with PYTHIA6.1 [20, 21]. The signal and background simulation used the package ATLFast [25] in order to simulate the response of the ATLAS detector.

4. The $H \rightarrow W^{(*)}W^{(*)} \rightarrow l^+l^-p_T$ Mode

A study of this mode at hadron level followed by a fast simulation of the ATLAS detector was first performed in [26]. In this Section we report on a re-analysis over a broader mass range $115 < M_H < 500$ GeV. Additionally, the treatment of the main background process is improved in the present analysis.

4.1 Background Generation

4.1.1 $t\bar{t}$ Production Associated with Jets

The production of $t\bar{t}$ associated with one jet, $t\bar{t}j$, was identified as the main background process for this mode [15, 16]. Early parton level analyses were based on $t\bar{t}j$ Leading Order (LO) Matrix Element (ME) calculation. In order to assess hadronization and detector effects, it is necessary to interface the fixed order ME calculations with a parton shower in a consistent way. Here we use a Next-to-Leading-Order

¹The central jet and b-jet vetoes are applied if a jet (b-jet) with $P_T > 20$ GeV is found in the range $|\eta| < 3.2$ and $|\eta| < 2.5$, respectively.

²The results from PYTHIA agree with the calculation provided by VV2H [22] by better than 3%.

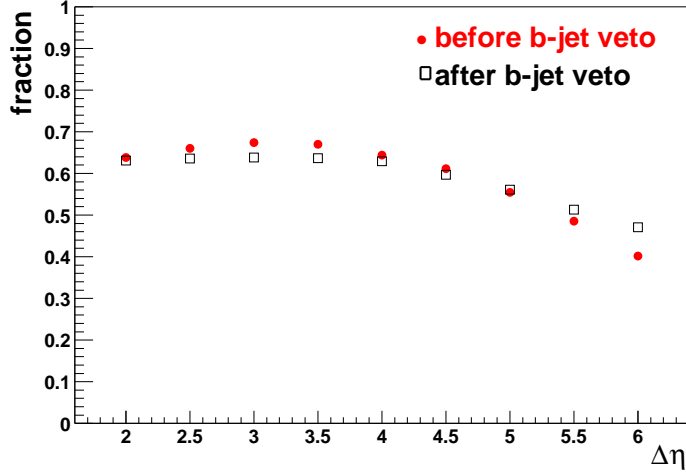


Fig. 1: Fraction of events for which either the leading or the sub-leading jet is a b-jet as a function of the cut on $\Delta\eta_{j_1 j_2}$ before and after the application of a b-jet veto.

description of the $t\bar{t}$ ME matched with parton shower provided within the MC@NLO package, which avoids double-counting and allows for a smooth matching between hard and soft/collinear emission regions [27, 28]. In MC@NLO hard emissions are treated as in NLO calculations while soft/collinear emissions are handled by the MC simulation (HERWIG6.5 in this case) with the MC logarithmic accuracy: the $t\bar{t}$ rates are known to NLO while the parton shower part preserves unitarity. Comparisons between MC@NLO and LO event generators PYTHIA6.2 [20, 21] and HERWIG6.5 [29, 30] show that, within the MC@NLO approach, the low P_T region is dominated by the parton shower prescription, while at higher P_T the NLO calculation dominates predicting a significantly higher P_T for the $t\bar{t}$ system.

PYTHIA6.2 predicts a softer P_T distribution with strong differences in the high P_T region ($P_T > 100$ GeV) with respect to the NLO prediction. It was also found that all three models give similar b-jet P_T distribution.

The MC@NLO description of the second jet from the $t\bar{t}jj$ process was tested against a LO $t\bar{t}jj$ ME calculation using MadGraphII [31, 32] interfaced to HERWIG6.5 [33]. To reduce the double-counting in the HERWIG6.5 interface with MadGraphII, the parton shower cutoff was set to the P_T of the lowest P_T QCD parton in the ME calculation. The resulting P_T distribution comparison showed that MC@NLO predicts a sub-leading non-b jet which is in good agreement for $P_T > 50$ GeV with the MadGraphII $t\bar{t}jj$ ME calculation. In conclusion, MC@NLO also provides a reasonable description of the sub-leading radiation.

MC@NLO was used to define a $t\bar{t}j$ control sample via an event selection similar to the one used in [15, 16, 17, 18]. The dependence of various kinematic distributions on $\Delta\eta_{j_1 j_2}$ was evaluated. In a large fraction ($\simeq 20\%$) of events with small values of $\Delta\eta_{j_1 j_2}$, both leading jets are b-jets. For $\Delta\eta_{j_1 j_2} > 3.5$ about 65% of the events have just one of the two leading jets being a b-jet (see Figure 1). This fraction is clearly dominated by $t\bar{t}j$ where the extra jet is hard. The rest of the events were examined and about 30% were found to have two leading jets that are non-b-jets. These events are dominated by $t\bar{t}jj$ where the two radiated partons are hard.

The results presented here show a small dependence of the jet topology on the b-jet veto. Only the third most energetic jet is affected but the reduction of the fraction of events for which the third jet is a b-jet is nearly constant as a function of the cut on $\Delta\eta_{j_1 j_2}$. According to these results, it is possible to define a control sample in the early stages of data taking with ATLAS to study properties of the $t\bar{t}$ process (for instance, normalization, central jet veto, b-jet veto). One would like to use the part of the phase space which is dominated by $t\bar{t}j$ and this is clearly the region for which the separation of the tagging jets is

Cut	VBF	$t\bar{t}$	EW WW	QCD WW	EW Zjj	QCD Zjj
a	33.2	3.34×10^3	18.2	670	11.6	2.15×10^3
b	13.1	128	11.1	3.58	3.19	66.9
c	12.4	117	10.5	3.31	1.13	19.6
d	10.1	85.1	7.74	0.95	0.96	8.55
e	7.59	13	5.78	0.69	0.90	6.01
f	5.67	2.26	1.03	0.16	0.27	0.92
g	4.62	1.12	0.44	0.1	0.01	0.02

Table 3: Cut flow for $M_H = 160$ GeV in the $e - \mu$ channel. Effective cross-sections are given in fb. The event selection presented in Section 4.2 is used. MC@NLO was used to estimate the contribution from $t\bar{t}$ production (see Section 4.11)

$\Delta\eta_{j_1 j_2} \gtrsim 3.5$. For a $< 10\%$ systematic error in the normalization of the $t\bar{t}j$ background about $300 - 500$ pb^{-1} of integrated luminosity will be needed.³

4.12 Other Background Processes

Other background processes were considered [19]:

- Electro-weak $WWjj$ production; a quark scattering process mediated by a vector boson, where the W bosons are produced and decay leptonically. This process is the second-dominant background for most masses. To model this process, we use a ME [35] that has been interfaced to PYTHIA6.1 [36].
- QCD $WWjj$ production. For this process, we use the generator provided in PYTHIA6.1.
- Electro-weak Zjj production. A Z boson is produced in a weak-boson-mediated quark-scattering process and decays into τ 's, which in turn decay leptonically. This process was modelled using a LO ME from the MadCUP project [37].
- QCD Zjj production. For this process, we use a LO ME from the MadCUP project. As before, we consider events where $Z \rightarrow \tau^+ \tau^-$, $\tau \rightarrow l\nu\nu$.
- QCD Zjj production with $Z \rightarrow l^+ l^-$ and $l = e, \mu$. This background can be reduced substantially by requiring a minimum missing P_T . However, it cannot be ignored because of its large cross-section. We model this process with the generator provided within PYTHIA6.1.⁴

4.2 Event Selection

Our procedure for optimizing the cuts is as follows: Begin with a set of loose (pre-selection) cuts and choose cuts on $\Delta\eta_{j_1 j_2}$, $\Delta\eta_{ll}$, $\Delta\phi_{ll}$, $M_{j_1 j_2}$, M_{ll} , and the transverse mass, M_T ,⁵ that optimize S/\sqrt{B} , where S and B are the expected number of signal and background events for 30 fb^{-1} of luminosity, respectively. We perform this optimization with a genetic algorithm [38]. We perform this procedure for several masses and find a parametrization for the optimal cut as a function of the Higgs mass.

The following event selection was chosen:

- Topology cuts. Require two charged leptons (e, μ) that pass the single or double charged lepton trigger in ATLAS. Here, a veto on b-jets is applied (see Section 2. and [19]).
- Forward jet tagging with $P_{Tj_1}, P_{Tj_2} > 20$ GeV and $\Delta\eta_{j_1 j_2}^{min} < \Delta\eta_{j_1 j_2}$ according to

$$\Delta\eta_{j_1 j_2}^{min} = \frac{a}{(M_H - b)} + cM_H + d, \quad (1)$$

³More details on this work are available in [34].

⁴In the final version of this work this process will be treated with a LO ME provided within MadCUP.

⁵The transverse mass is defined as in [15, 16, 17, 18].

where $a = 2861$, $b = -327$, $c = 9.6 \times 10^{-3}$, and $d = -3.44$. Leptons are required to be in between jets in pseudorapidity.

- c. Tau rejection [15, 16, 17, 18, 19].
- d. Tagging jets invariant mass: $520 \text{ GeV} < M_{j_1 j_2} < 3325 \text{ GeV}$
- e. Central jet veto (see Section 2. and [19]).
- f. Lepton angular cuts: We require $\Delta\eta_{ll} < \Delta\eta_{ll}^{max}$ with

$$\Delta\eta_{ll}^{max} = a + bM_H + cM_H^2, \quad (2)$$

where $a = 6.25$, $b = -6.24 \times 10^{-2}$, $c = 1.99 \times 10^{-4}$ for $M_H < 200 \text{ GeV}$, and $a = 3.88$, $b = -4.17 \times 10^{-3}$, $c = 0$ for $M_H > 200 \text{ GeV}$. It is required that $\Delta\phi_{ll}^{min} < \Delta\phi_{ll} < \Delta\phi_{ll}^{max}$ with

$$\Delta\phi_{ll}^{min} = a + bM_H, \quad (3)$$

where $a = -2.20$, $b = 7.54 \times 10^{-3}$, and

$$\Delta\phi_{ll}^{max} = a + bM_H + cM_H^2 + dM_H^3, \quad (4)$$

where $a = -4.07$, $b = 0.156559$, $c = -1.310956 \times 10^{-3}$, and $d = 3.42011 \times 10^{-6}$. As one would expect, the minimum cut is only important at high Higgs masses, and the upper bound is only relevant at low Higgs masses. It is required that $M_{ll}^{min} < M_{ll} < M_{ll}^{max}$ with

$$M_{ll}^{min} = a(M_H - b)^2 + c, \quad (5)$$

where $a = -2.82 \times 10^{-3}$, $b = 464$, $c = 129$, and

$$M_{ll}^{max} = \frac{a(M_H - b)^2}{d + (M_H - b)^2} + c, \quad (6)$$

where $a = 310$, $b = 114$, $c = 47.6$, and $d = 13290$. In order to further reduce the contribution from Drell-Yan, we require $85 < M_{ll} < 95 \text{ GeV}$ and $\cancel{p}_T > 30 \text{ GeV}$, if leptons are of same flavor.

- g. Transverse mass cuts. We require that $M_T^{min} < M_T < M_T^{max}$, with

$$M_T^{min} = a + bM_H, \quad (7)$$

where $a = -17$ and $b = 0.73$ and

$$M_T^{max} = a + bM_H + cM_H^2 + dM_H^3, \quad (8)$$

where $a = 106$, $b = -0.83$, $c = 9.46 \times 10^{-3}$, and $d = -9.49 \times 10^{-6}$. We also require $m_T(ll\nu\nu) > 30 \text{ GeV}$, with $m_T(ll\nu\nu) = \sqrt{2P_T^{ll}\cancel{p}_T(1 - \cos \Delta\phi)}$, where P_T^{ll} is the P_T of the dilepton system and $\Delta\phi$ corresponds to the angle between the di-lepton vector and the \cancel{p}_T vector in the transverse plane.

4.3 Results and Discovery Potential

Table 3 displays effective cross-sections for signal and background after application of successive cuts presented in Section 4.2. Cross-sections are presented for $M_H = 160 \text{ GeV}$ in the $e - \mu$ channel. It is worth noting that the central jet veto survival probability for $t\bar{t}$ production is significantly lower than that reported in [19]. However, this is compensated by a lower rejection due to requiring two tagging jets (see cut **b** in the previous Section). As a result, the relative contribution to the background from $t\bar{t}$ production obtained here is similar to the one reported in [19]. Table 4 reports the expected Poisson significance for 10 fb^{-1} of integrated luminosity. Simple event counting is used and a 10% systematic error on the background determination was assumed. In order to incorporate the systematic errors we incorporated [39, 40] the formalism developed in [41]. The implementation of MC@NLO to simulate the $t\bar{t}$ background has not changed the conclusions drawn in [19] for the M_H considered there. The $H \rightarrow W^{(*)}W^{(*)} \rightarrow l^+l^-\cancel{p}_T$ mode has a strong potential in a wide range of Higgs masses. A significance of or greater than 5σ may be achieved with 30 fb^{-1} of integrated luminosity for $125 < M_H < 300 \text{ GeV}$.

$M_H(\text{GeV})$	$e - \mu$	$e - e$	$\mu - \mu$	Combined
115	0.9	0.4	0.5	1.4
130	3.0	1.5	2.2	4.3
160	8.2	5.1	6.3	11.6
200	4.4	2.6	3.0	6.0
300	2.3	1.4	1.5	3.1
500	1.0	0.6	0.6	1.5

Table 4: Expected Poisson significance for the parameterized cuts listed in Section 4.2 with 10 fb^{-1} of integrated luminosity. A 10% systematic uncertainty is applied to all backgrounds when calculating the significance.

5. The $H \rightarrow \gamma\gamma$ Mode

5.1 Generation of Background Processes

The relevant background processes for this mode are subdivided into two major groups. Firstly, the production of two γ 's associated with two jets (real photon production). Secondly, a sizeable contribution is expected from events in which at least one jet is misidentified as a photon (fake photon production). Despite the impressive jet rejection rate after the application of γ selection criteria expected to be achieved by the ATLAS detector [11] ($\gtrsim 10^3$ for each jet), the contribution from fake photons will not be negligible due to the large cross-sections of QCD processes at the LHC.

LO ME based MC's were used to simulate $\gamma\gamma jj$ (both QCD and EW diagrams), γjjj and $jjjj$ production. For this purpose MadGraphII [31, 32] interfaced with PYTHIA6.2 was used [33]. The factorization and re-normalization scales were set to the P_T of the lowest P_T parton.

After the application of a number of basic cuts at the generator level (see [42]) the QCD and EW γjjj diagrams correspond to 6.32 nb and 1.21 pb, respectively. Assuming an effective jet rejection of the order of 10^3 , the starting cross-section for the EW γjjj process would be about 1 fb. This small cross-section will be severely reduced after the application of further selection cuts (see Section 5.2). In the analysis EW γjjj and $jjjj$ diagrams were neglected.⁶

5.2 Event Selection

A number of pre-selection cuts are applied which are similar to those used in the multivariate analysis of VBF $H \rightarrow W^{(*)}W^{(*)} \rightarrow l^+l^- \cancel{p}_T$ [43]:

- a. $P_{T\gamma 1}, P_{T\gamma 2} > 25 \text{ GeV}$. The γ 's are required to fall in the central region of the detector excluding the interface between the barrel and end-cap calorimeters ($1.37 < |\eta| < 1.52$). The latter requirement reduces the acceptance by about 10%.
- b. Tagging jets with $P_{Tj_1}, P_{Tj_2} > 20 \text{ GeV}$ and $\Delta\eta_{j_1j_2} > 3.5$.
- c. The γ 's should be in between the tagging jets in pseudorapidity.
- d. Invariant mass of the tagging jets, $M_{j_1j_2} > 100 \text{ GeV}$.
- e. Central jet veto [19].
- f. Invariant mass window: $M_H - 2 \text{ GeV} < M_{\gamma\gamma} < M_H + 2 \text{ GeV}$.

The final event selection is obtained by means of maximizing the Poisson significance for 30 fb^{-1} of integrated luminosity for $M_H = 120 \text{ GeV}$. The maximization procedure is performed with the help of the MINUIT program [44]. The following variables are chosen: $P_{Tj_1}, P_{Tj_2}, \Delta\eta_{j_1j_2}, \Delta\phi_{j_1j_2}, M_{j_1j_2}, P_{T\gamma 1}, P_{T\gamma 2}$, and $\Delta\eta_{\gamma\gamma}$.

Due to the implementation of parton shower and hadronization effects, the kinematics of the final state will be somewhat different from that of the parton level analysis performed in [45]. After the

⁶More details of MC generation for background processes are available in [42].

Cut	Pre-selection	Parton Level	Optimization
a	$P_{T\gamma_1}, P_{T\gamma_2} > 25 \text{ GeV}$	$P_{T\gamma_1} > 50 \text{ GeV}$ $P_{T\gamma_2} > 25 \text{ GeV}$	$P_{T\gamma_1} > 57 \text{ GeV}$ $P_{T\gamma_2} > 34 \text{ GeV}$ $\Delta\eta_{\gamma\gamma} < 1.58, \Delta\phi_{\gamma\gamma} < 3 \text{ rad}$
b	$P_{Tj_1}, P_{Tj_2} > 20 \text{ GeV}$ $\Delta\eta_{j_1j_2} > 3.5$	$P_{Tj_1} > 40 \text{ GeV}$ $P_{Tj_2} > 20 \text{ GeV}$ $\Delta\eta_{j_1j_2} > 4.4$	$P_{Tj_1} > 40 \text{ GeV}$ $P_{Tj_2} > 29.5 \text{ GeV}$ $\Delta\eta_{j_1j_2} > 3.9$
d	$M_{j_1j_2} > 100 \text{ GeV}$	-	$M_{j_1j_2} > 610 \text{ GeV}$

Table 5: Values of the cuts applied for different event selections (see Section 5.2).

application of cut **f** in the pre-selection, the dominant background corresponds to QCD $\gamma\gamma jj$ and the fake photon production, therefore, the optimization process will be mainly determined by the kinematics of these process together with that of the VBF signal.

Initially, it has been verified that the inclusion of variables additional to those considered in [45] improves the signal significance. The addition of the photon related variables $\Delta\eta_{\gamma\gamma}$ and $\Delta\phi_{\gamma\gamma}$ improves the signal significance by some 10 – 20% depending on the Higgs mass. The implementation of those two variables separately proves more efficient than the combined $\Delta R_{\gamma\gamma}$. The inclusion of the hadronic variable $\Delta\phi_{jj}$ does not noticeably increase the signal significance.

Table 5 shows the results of the optimization together with the values of the cuts placed at the pre-selection level and for the parton level analysis performed in [45]. Due to the significant increase in the background contribution compared to the parton level analysis, the optimized event selection is significantly tighter, resulting into reduced signal and background rates (see Section 5.3). The increase of the background comes from the different choice of the width of the mass window, the implementation of parton showers for the estimation of the central jet veto probability and the inclusion of fake photon events.

5.3 Results and Discovery Potential

Here, we use the event selection obtained in the optimization procedure performed in Section 5.2 (see Table 5). The expected signal and background cross-sections corrected for acceptance and efficiency corrections are shown in Table 6 for a mass window around $M_H = 120 \text{ GeV}$ after the application of successive cuts.

The contribution from the fake photon background has been severely reduced thanks to the inclusion of the photon angular variables. The contribution from this background, however, is important. The normalization of the fake photon background is subject to sizeable systematic uncertainties. This is partly due to the uncertainty on the determination of the fake photon rejection rate [11].

Figure 2 shows the expected signal and background effective cross-section (in fb) as a function of $M_{\gamma\gamma}$ for $M_H = 130 \text{ GeV}$. The dashed line shows the total background contribution whereas the dotted line corresponds to the real $\gamma\gamma$ background. The solid line displays the expected contribution of signal plus background. In Table 7, results are given in terms of S and B , for 30 fb^{-1} of integrated luminosity. The signal significance was calculated with a Poissonian calculation. The signal significance expected with this VBF mode alone reaches 2.2σ for 30 fb^{-1} of integrated luminosity.

The QCD $\gamma\gamma jj$ has been estimated with QCD $\gamma\gamma jj$ ME based MC alone. The rate of additional (non tagging) jets has been estimated with the help of the parton shower. This approach yields a central jet veto survival probability significantly smaller than that calculated in [45]. Both effects go in the direction of overestimating of the $\gamma\gamma jj$ background. Similar discussion applies to the estimation of the fake photon background performed here. This background estimation may be improved with the

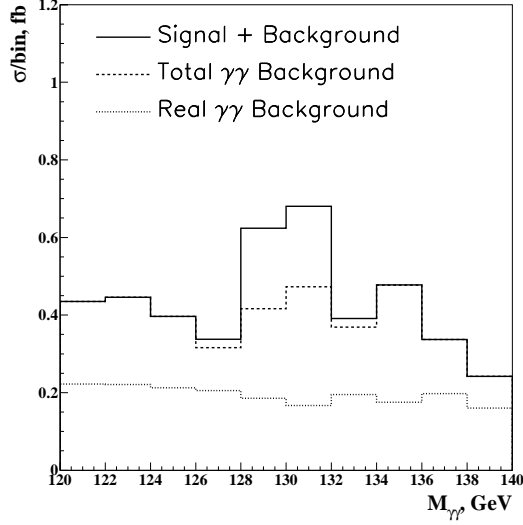


Fig. 2: Expected signal and background effective cross-section (in fb) as a function of $M_{\gamma\gamma}$ for $M_H = 130$ GeV. The dashed line shows the total background contribution whereas the dotted line corresponds to the real $\gamma\gamma$ background. The solid line displays the expected contribution of signal plus background.

Cut	VBF H	g-g Fusion H	QCD $\gamma\gamma jj$	EW $\gamma\gamma jj$	γjjj	$jjjj$
a	2.25	5.45	246.90	7.97	172.60	691.06
b	0.73	0.08	31.83	4.39	28.30	35.22
c	0.70	0.07	16.81	4.20	21.76	30.06
d	0.57	0.04	7.43	3.69	12.77	16.99
e	0.42	0.02	5.41	2.50	8.52	8.49
f	0.38	0.02	0.28	0.14	0.22	0.25

Table 6: Expected signal and background cross-sections (in fb) corrected for acceptance and efficiency corrections after the application of successive cuts (see Section 5.2). Here $M_H = 120$ GeV.

implementation of a more realistic MC for the simulation of the real photon background. This mode is considerably more sensitive to the understanding of fake photon rejection than the inclusive analysis [11].

6. The $H \rightarrow ZZ \rightarrow l^+l^-q\bar{q}$ Mode

6.1 Generation of Background Processes

Cross-section for the QCD $Z + 4j$, $Z \rightarrow l^+l^-$, $l = e, \mu$ process were calculated with two independent packages: ALPGEN [46] and MadGraphII [31, 32]. Both calculations include the Z/γ^* interference effects. The following cuts at the generator level were used for the cross-section calculation for the nominal event generation:

- QCD parton's transverse momentum, $P_T > 20$ GeV, pseudorapidity, $|\eta| < 5$. Separation between QCD partons, $\Delta R > 0.5$.
- Minimal transverse momentum cuts on leptons, $P_T > 3$ GeV with $|\eta| < 3$. The angle separation between leptons and leptons and jets were set to $\Delta R > 0.2$

The Born level cross-section of QCD $Z + 4j$ production is subject to large uncertainties. Some properties of jets in association with W and Z bosons have been studied and have been compared with QCD predictions at the Tevatron [47, 48]. The measured cross-sections of $W/Z + n$ jets where $n = 1, 2, 3, 4$ lie in between the LO predictions calculated using the re-normalization and factorization scales

M_H	S	B	S/B	σ_P
110	10.05	30.69	0.33	1.56
120	12.06	26.54	0.45	2.02
130	12.52	23.97	0.52	2.19
140	10.91	22.90	0.48	1.94
150	7.69	20.15	0.38	1.42
160	2.89	17.21	0.17	0.44

Table 7: Expected number of signal and background events, S/B and the corresponding signal significance for 30 fb^{-1} of integrated luminosity (see Section 5.3).

equal to the average transverse momentum of the partons, $\langle P_T \rangle$, and the transverse energy of the weak boson, E_T^{WB} , respectively. The LO prediction calculated with the first choice of scale systematically undershoots the measured cross-section. At the LHC $\langle P_T \rangle > 100 \text{ GeV}$, due to the large phase space. Thus, the scale was set to the mass of the weak boson.

After the application of the cuts at the generator level and the choice of scales mentioned above both ALPGEN and MadGraphII yield 47.5 pb . 8.5 million un-weighted events were generated with MadGraphII. The output from MadGraphII was interfaced to the HERWIG6.5 package [33]. In order to avoid severe double counting in the generation of hadronic jets, the scale of the parton shower evolution was set to the P_T of the lowest transverse momentum parton in the event.

The cross-section for $Z + 4j$, $Z \rightarrow l^+l^-$, $l = e, \mu$ production with one EW boson in the internal lines was evaluated with MadGraphII. These diagrams include QCD $ZZjj$ and $ZW^\pm jj$. A cross-section of 1.6 pb was obtained after cuts at generator level and by applying the same choice of scales as for the QCD $Z + 4j$ case. The impact of these diagrams is small, hence, they were not included in the final results reported in Section 6.3. Diagrams with two EW bosons in the internal lines were not considered, as they are expected to be negligible.

A sample of events for $t\bar{t}$ production was used. These events were generated with the MC@NLO package (see Section 4.1).

6.2 Event Selection

The event selection presented in this Section is obtained by maximizing the signal significance for a Higgs for $M_H = 300 \text{ GeV}$ with 30 fb^{-1} of integrated luminosity.

A number of basic features common to VBF modes remain. A feature specific to the mode under study is the additional ambiguity in the definition of tagging jets introduced by the presence of relatively hard jets produced from the decay of the Z 's. A search for two jets with an invariant mass close to Z mass, M_Z , is performed. After reconstructing the Z decaying hadronically, the event looks like a ‘‘typical’’ VBF candidate.

The following event selection was chosen:

- a. Two isolated, oppositely charged, of equal flavor leptons in the central detector region, $|\eta| < 2.5$.
- b. The event is required to pass the single or double lepton trigger in ATLAS.
- c. Two hadronic jets (j_3, j_4) with transverse momentum, $P_T > 30 \text{ GeV}$ with $M_{j_3j_4}$ close to M_Z were required in the fiducial region of the calorimeter, $|\eta| < 4.9$. The relative invariant mass resolution of two jets is expected to be approximately 10%. The following mass window was chosen: $75 < M_{j_3j_4} < 101 \text{ GeV}$. These jets were ‘‘masked out’’ from the list of jets.
- d. Tagging jets with $P_{Tj_1} > 40 \text{ GeV}$, $P_{Tj_2} > 30 \text{ GeV}$ and $\Delta\eta_{j_1j_2} > 4.4$.
- e. Both leptons were required to lie in between the tagging jets in pseudorapidity.

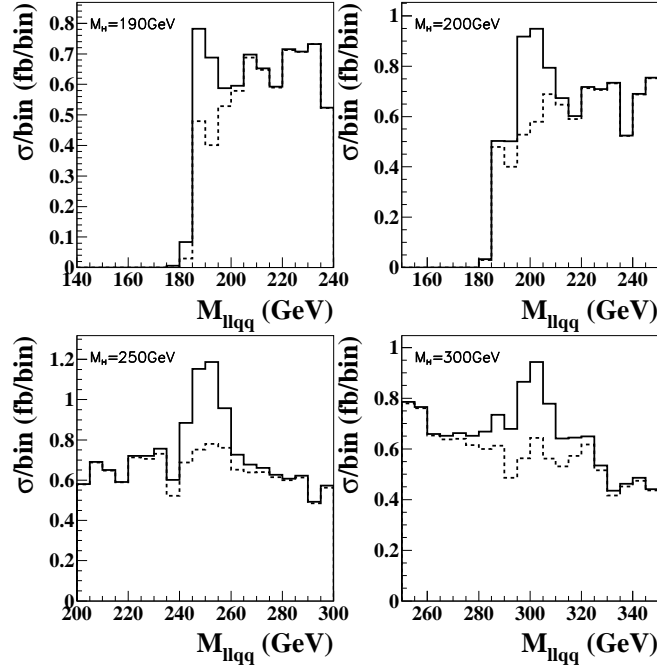


Fig. 3: Invariant mass of the Higgs candidates after the application of kinematic fits. The solid lines correspond to the sum of the signal (VBF $H \rightarrow ZZ \rightarrow l^+l^-q\bar{q}$) and the main background (QCD $Z + 4j$, $Z \rightarrow l^+l^-$, $l = e, \mu$). The dashed lines show the contribution of the main background alone. Here $M_H = 190, 200, 250, 300$ GeV.

- f. Leptonic cuts. It was required that $M_Z - 10 < M_{ll} < M_Z + 10$ GeV. This cut is expected to suppress di-lepton final states with $W^+W^- \rightarrow ll\nu\nu$. It is particularly important to suppress the contribution from $t\bar{t}$ production associated with jets. No b-tagging rejection algorithms were applied in this analysis due to the large branching ratio of Z decaying into heavy quarks.
- g. The invariant mass of the tagging jets was required to be greater than 900 GeV.
- h. Central jet veto. Extra jets with $P_T > 20$ GeV are looked for in the central region of the detector ($|\eta| < 3.2$). However, high P_T quarks from the decay of one of the Z 's are expected to radiate hard gluons with a high probability, thus, faking hadronic jets produced prior to the decay. If ΔR between the extra jet and the jets of the Higgs candidate is larger than one unit, the event is vetoed.
- i. In order to further reduce the contribution from events with $W^+W^- \rightarrow ll\nu\nu$, it is required that $\cancel{p}_T < 30$ GeV.

The $M_{llj_3j_4}$ spectrum could be distorted due to the ambiguity in defining tagging jets. The distortion of the $M_{llj_3j_4}$ spectrum, however, is not sizeable. Figure 3 displays the $M_{llj_3j_4}$ spectra for signal and background after the application of the event selection presented in this Section. A Higgs mass resolution of approximately 2.5% is obtained for $2M_Z < M_H < 300$ GeV [49].

6.3 Results and Discovery Potential

Table 8 shows the expected signal effective cross-sections (in fb) for a Higgs mass of $M_H = 300$ GeV. Table 8 also displays the effective cross-sections for the major background processes. Cross-sections are given after successive cuts (see Section 6.2). The background is largely dominated by the QCD $Z + 4j$, $Z \rightarrow l^+l^-$, $l = e, \mu$ production. Diagrams with one or two EW boson in the internal lines were neglected. The contribution from $t\bar{t}$ is small and it is also neglected in the final results.

Table 9 reports results in terms of S , B , S/B and signal significance, σ_L , with 30 fb^{-1} of integrated luminosity for different values of M_H . The effective signal and background cross-sections are evaluated in a $4\sigma_M$ (where σ_M is the mass resolution) wide mass window. The signal significance was

Process	a	b	c	d	e	f	g	h	i
VBF ($M_H = 300$ GeV)	31.69	31.50	12.63	3.39	3.26	2.93	2.24	1.72	1.66
QCD $Z + 4j$	25930	25902	10345	277	205	205	116	36.6	34.6
$t\bar{t}$	14793	14268	4233	135	106	10.5	6.4	2.3	0.3

Table 8: Expected effective cross-sections (in fb) for $H \rightarrow ZZ \rightarrow llq\bar{q}$ produced via VBF ($M_H = 300$ GeV) and the main background processes. Cross-sections are given after successive cuts presented in Section 6.2.

M_H (GeV)	S	B	S/B	σ_L
190	18.9	31.2	0.61	3.47
200	27.3	52.8	0.52	3.76
300	39.3	116.1	0.34	3.75
500	20.1	124.2	0.16	1.98

Table 9: Expected number of signal and background events, ratio of signal to background and signal significance (in σ) for a SM Higgs produced via VBF using the decay mode $H \rightarrow ZZ \rightarrow l^+l^-q\bar{q}$ with 30 fb^{-1} of integrated luminosity for different values of M_H . The effective signal and background cross-sections are evaluated in a $4\sigma_M$ (where σ_M is the mass resolution) wide mass window. The signal significance, σ_L , was calculated with a likelihood ratio technique using the invariant mass of the Higgs candidate as a discriminant variable.

calculated with a likelihood ratio technique using the invariant mass of the Higgs candidate as a discriminant variable [39, 40]. A signal significance of 3.75σ may be achieved for $M_H = 300$ GeV with 30 fb^{-1} of integrated luminosity. It should be noted that the cross-sections for the main background reported here are subject to large theoretical uncertainty. Fortunately, the background may be determined from side bands for Higgs searches with $M_H > 200$ GeV.

7. Multivariate Analysis

Results reported in [19] and the present paper were based on classical cut analyses. Multivariate techniques have been extensively used in physics analyses, for instance, in LEP experiments. Neural Networks (NN) are the most commonly used tools in multivariate analyses. NN training has been performed on the $H \rightarrow W^{(*)}W^{(*)} \rightarrow l^+l^-p_T$ [43] and $H \rightarrow \tau^+\tau^- \rightarrow l^+l^-p_T$ [50] modes. NN training was performed with a relatively small number of variables. It was required that these variables are infrared safe and their correlations do not depend strongly on detector effects: $\Delta\eta_{j_1j_2}$, $\Delta\phi_{j_1j_2}$, $M_{j_1j_2}$, $\Delta\eta_{ll}$, $\Delta\phi_{ll}$, M_{ll} , and M_T (or the invariant mass of the $\tau^+\tau^-$ system in the case of the $H \rightarrow \tau^+\tau^- \rightarrow l^+l^-p_T$ mode). The signal significance was calculated with a likelihood ratio technique using the NN output as a discriminant variable. An enhancement of approximately 30 – 50% of the signal significance with respect to the classical cut analysis was obtained for both modes under consideration.

8. Conclusions

The discovery potential for the SM Higgs boson produced with VBF in the range $115 < M_H < 500$ GeV has been reported. An updated study at hadron level followed by a fast detector simulation of the $H \rightarrow W^{(*)}W^{(*)} \rightarrow l^+l^-p_T$ mode has been presented: the main background, $t\bar{t}$ associated with jets, has been modelled with the MC@NLO program and the Higgs mass range has been extended to 500 GeV. This mode has a strong potential: a signal significance of more than 5σ may be achieved with 30 fb^{-1} of integrated luminosity for $125 < M_H < 300$ GeV. The discovery potential of the $H \rightarrow \gamma\gamma$ and $H \rightarrow ZZ \rightarrow l^+l^-q\bar{q}$ modes have also been reported with analyses at hadron level followed by a fast detector simulation.

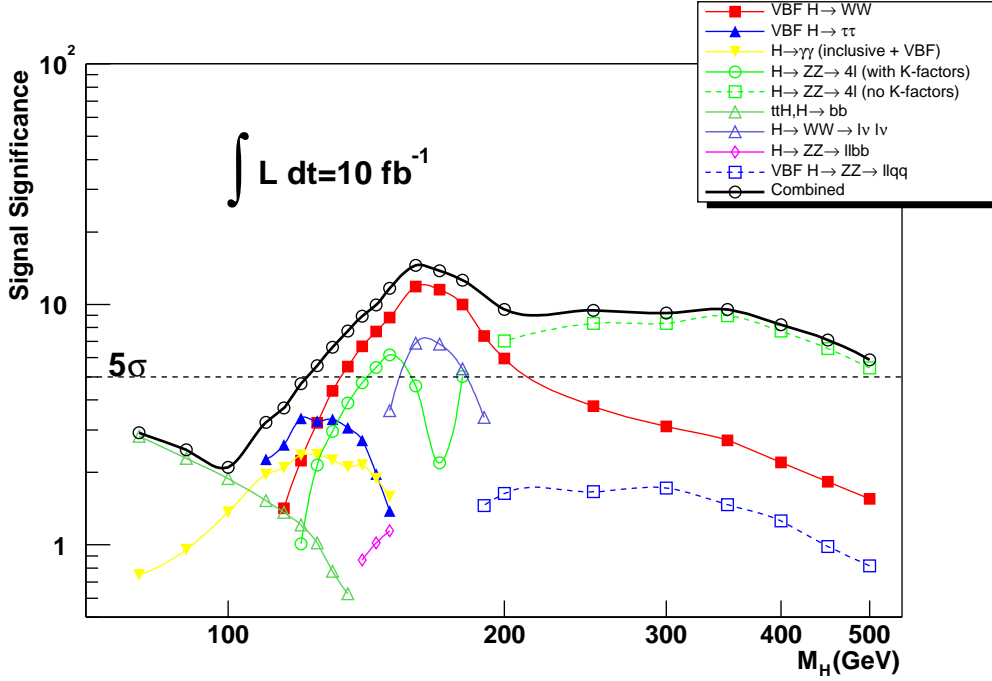


Fig. 4: Expected significance for ATLAS as a function of Higgs mass for 10 fb^{-1} of integrated luminosity.

The discovery potential of the modes presented in this work was combined with results reported in past studies performed for the ATLAS detector. Results from recent studies [51, 52, 53], which were not used in [19], were added here. Likelihood ratio techniques have been used to perform the combination [39, 40]. In order to incorporate systematic errors, the formalism developed in [41] was implemented. A 10 % systematic error on the background estimation has been assumed for modes related to VBF [19]. Figure 4 displays the overall discovery potential of the ATLAS detector with 10 fb^{-1} of integrated luminosity. Results from NN based analyses and discriminating variables have not been included in the combination. The present study confirms the results reported in [15, 16, 17, 18, 19], that the VBF mechanism yields a strong discovery potential at the LHC in a wide range of the Higgs boson mass.

9. Acknowledgements

We are particularly indebted to F. Cerutti, S. Frixione, K. Jakobs, T. Plehn, D. Rainwater, and D. Zeppenfeld. All of us would like to thank the organizers of the *Les Houches Workshop* for the fruitful workshop.

References

- [1] S. L. Glashow, Nucl. Phys. **B22** (1961) 579
- [2] S. Weinberg, Phys. Rev. Lett. **19** (1967) 1264
- [3] A. Salam, Proceedings to the Eighth Nobel Symposium, May 1968, ed: N. Svartholm (Wiley, 1968) 357
- [4] S.L. Glashow, J. Iliopoulos and L. Maiani, Phys. Rev. **D2** (1970) 1285
- [5] P.W. Higgs, Phys. Lett. **12** (1964) 132
- [6] P.W. Higgs, Phys. Rev. Lett. **13** (1964) 508
- [7] P.W. Higgs, Phys. Rev. **145** (1966) 1156
- [8] F. Englert, R. Brout, Phys. Rev. Lett. **13** (1964) 321
- [9] G.S. Guralnik, C.R. Hagen and T.W.B. Kibble, Phys. Rev. Lett. **13** (1964) 585
- [10] T.W.B. Kibble, Phys. Rev. **155** (1967) 1554
- [11] ATLAS Collaboration, Detector and Physics Performance Technical Design Report, CERN-LHCC/99-14 (1999)
- [12] H.M. Georgi, S.L. Glashow, M.E. Machacek and D.V. Nanopoulos, Phys. Rev. Lett. **40** (1978) 11
- [13] R. Cahn and S. Dawson, Phys. Lett. **B136** (1984) 196
- [14] G. Kane, W. Repko and W. Rolnick, Phys. Lett. **B148** (1984) 367
- [15] D.L. Rainwater and D. Zeppenfeld, Phys. Rev. **D60** (1999) 113004
- [16] N. Kauer, T. Plehn, D.L. Rainwater and D. Zeppenfeld, Phys. Lett. **B503** (2001) 113
- [17] T. Plehn, D.L. Rainwater and D. Zeppenfeld, Phys. Rev. **D61** (2000) 093005
- [18] D.L. Rainwater and D. Zeppenfeld, JHEP **9712** (1997) 005
- [19] S. Asai *et al.*, Search for the Standard Model Higgs Boson in ATLAS using Vector Boson Fusion, ATLAS Scientific Note SN-ATLAS-2003-024 (2003), submitted to EPJ, hep-ph/0402254
- [20] T. Sjöstrand, Comp. Phys. Comm. **82** (1994) 74
- [21] T. Sjöstrand *et al.*, Comp. Phys. Comm. **135** (2000) 238
- [22] M. Spira, VV2H Programe, home.cern.ch/m/mspira/www.proglist.html
- [23] H.L. Lai *et al.*, Eur. Phys. J. **C12** (2000) 375
- [24] A. Djouadi, J. Kalinowski and M. Spira, HDECAY: a Program for Higgs Boson Decays in the Standard Model and its Supersymmetric Extension, Comp. Phys. Comm. **108** (1998) 56
- [25] E. Richter-Was, D. Froidevaux and L. Poggioli, ATLFAST2.0 a Fast Simulation Package for ATLAS, ATLAS Note ATL-PHYS-98-131 (1998)
- [26] C. Buttar, K. Jakobs and R. Harper, Weak boson fusion H-WW(*)-l+l-Pt-miss as a search mode for an intermediate mass SM Higgs boson at ATLAS, ATLAS Note ATL-PHYS-2002-033 (2002)

- [27] S. Frixione and B.R. Webber, *JHEP* **0206** (2002) 029
- [28] S. Frixione and B.R. Webber, *JHEP* **0308** (2003) 007
- [29] G. Corcella *et al.*, *JHEP* **0101** (2001) 010
- [30] G. Corcella *et al.*, HERWIG 6.5: an Event Generator for Hadron Emission Reactions with Interfering Gluons, hep-ph/0011363
- [31] T. Stelzer and W.F. Long, *Phys. Comm.* **81** (1994) 357
- [32] F. Maltoni and T. Stelzer, MadEvent: Automatic Event Generation with MadGraph, hep-ph/0208156 (2002)
- [33] Wisconsin Higgs Project, Software web page, <http://www-wisconsin.cern.ch/physics/software.html>
- [34] Y.Q. Fang, B. Mellado, W. Quayle, S. Paganis and Sau Lan Wu, A Study of the $t\bar{t}+jets$ background at LHC, ATLAS internal Communication ATL-COM-PHYS-2003-043 (2003)
- [35] D. Zeppenfeld, private communication
- [36] R. Mazini, private communication
- [37] D. Zeppendeld *et al.*, The Madison Collection of User Processes, <http://pheno.physics.wisc.edu/Software/MadCUP/>
- [38] M. Wall, GALib: A C++ Library of Genetic Algorithm Components, <http://lancet.mit.edu/ga/>
- [39] K. Cranmer, B. Mellado, W. Quayle and Sau Lan Wu, Confidence Level Calculations in the Search for Higgs Bosons Decay $H \rightarrow W^+W^- \rightarrow l^+l^- \cancel{p}_T$ Using Vector Boson Fusion, ATLAS Note ATL-PHYS-2003-008 (2003)
- [40] K. Cranmer, B. Mellado, W. Quayle and Sau Lan Wu, Challenges of Moving the LEP Higgs Statistics to the LHC, physics/0312050 (2003)
- [41] R.D. Cousins and V.L. Highland, *Nucl. Instrum. Methods* **A320** (1992) 331
- [42] K. Cranmer, B. Mellado, W. Quayle and Sau Lan Wu, Search for Higgs Boson Decay $H \rightarrow \gamma\gamma$ Using Vector Boson Fusion, ATLAS Note ATL-PHYS-2003-036 (2003), hep-ph/0401088
- [43] K. Cranmer, B. Mellado, W. Quayle and Sau Lan Wu, Neural Network Based Search for Higgs Boson Produced via VBF with $H \rightarrow W^+W^- \rightarrow l^+l^- \cancel{p}_T$ for $115 < M_H < 130$ GeV, ATLAS Note ATL-PHYS-2003-007 (2003)
- [44] F. James and M. Roos, *Comp. Phys. Comm.* **10** (1975) 343
- [45] D.L. Rainwater, Intermediate-Mass Higgs Searches in Weak Boson Fusion, Ph.D. thesis, University of Wisconsin - Madison, 1999
- [46] M.L. Mangano *et al.*, ALPGEN, a Generator for Hard Multiparton Processes in Hadronic Collisions, hep-ph/0206293 (2002)
- [47] CDF Collaboration, F. Abe *et al.*, *Phys. Rev. Lett.* **77** (1996) 448
- [48] CDF Collaboration, F. Abe *et al.*, *Phys. Rev. Lett.* **79** (1997) 4760

- [49] K. Cranmer, B. Mellado, W. Quayle and Sau Lan Wu, Search for Higgs Boson Decay $H \rightarrow ZZ \rightarrow l^+l^-qq, l = e, \mu$ with $2 \cdot M_Z < M_H < 500$ GeV Using Vector Boson Fusion, ATLAS internal Communication ATL-COM-PHYS-2003-035 (2003)
- [50] K. Cranmer, B. Mellado, W. Quayle and Sau Lan Wu, Neural Network Based Search for Higgs Boson Produced via VBF with $H \rightarrow \tau^+\tau^- \rightarrow l^+l^-p_T$, ATLAS Note, in preparation
- [51] G. Martinez, E. Gross, G. Mikenberg and L. Zivkovic, Prospects for Light Higgs Observation in the $H^0 \rightarrow Z^0Z^{0*} \rightarrow b\bar{b}ee(\mu\mu)$ Channel at the LHC, ATLAS Note ATL-PHYS-2003-001 (2003)
- [52] J. Cammin and M. Schumacher, The ATLAS Discovery Potential for the Channel ttH, H to bb, ATLAS Note ATL-PHYS-2003-024 (2003)
- [53] K. Cranmer, B. Mellado, W. Quayle and Sau Lan Wu, Application of K Factors in the $H \rightarrow ZZ^* \rightarrow 4l$ Analysis at the LHC, ATLAS Note ATL-PHYS-2003-025 (2003), hep-ph/0307242.